Geomechanics and Geoengineering
An International Journal

ISSN: (Print) (Online) Journal homepage: https://www.tandfonline.com/loi/tgeo20

Artificial neural networks to predict deformation modulus of rock masses considering overburden stress

K. Tokgozoglu, C. H. Aladag & C. Gokceoglu

To cite this article: K. Tokgozoglu, C. H. Aladag & C. Gokceoglu (2021): Artificial neural networks to predict deformation modulus of rock masses considering overburden stress, Geomechanics and Geoengineering, DOI: 10.1080/17486025.2021.2008518

To link to this article: https://doi.org/10.1080/17486025.2021.2008518

Published online: 28 Nov 2021.

GEOMECHANICS AND GEOENGINEERING
https://doi.org/10.1080/17486025.2021.2008518

Taylor & Francis
Taylor & Francis Group

Artificial neural networks to predict deformation modulus of rock masses considering overburden stress

K. Tokgozoglu [a], C. H. Aladag [b] and C. Gokceoglu [c]

[a]Geological and Geotechnical Division, Yuksel Proje Co, Ankara, Turkey; [b]Department of Statistics, Hacettepe University, Ankara, Turkey; [c]Department of Geological Engineering, Hacettepe University, Ankara, Turkey

ABSTRACT

The effect of overburden stress on the rock mass deformation modulus is a known issue. However, the effect of overburden stress has been studied less with empirical methods due to the lack of appropriate data. In this study, it is aimed to investigate the effect of overburden stress on rock mass deformation modulus using artificial neural network (ANN). Four ANN models have been developed in accordance with the purpose of the study. Two of these models do not contain the overburden stress parameter, but the other two models contain the overburden stress parameter. The prediction performance of the models containing the overburden stress parameter was obtained drastically higher than the others. In other words, the value account for (VAF) and root-mean-square error (RMSE) indices of the model having the inputs of rock mass rating (RMR) and elasticity modulus of intact rock (E_i) are 73.3% and 462, respectively, while those of the model having the inputs of RMR, E_i and overburden stress are 90% and 265. The other models developed in the present study yielded similar results. Consequently, with the ANN models developed in this study, the effect of overburden stress on E_m is revealed, clearly.

ARTICLE HISTORY
Received 27 July 2021
Accepted 15 November 2021

KEYWORDS
Deformation modulus; rock mass; intact rock; ANN; overburden stress

Introduction

The deformation modulus of rock masses is one of the most important parameters used in the design of any engineering structure to be constructed in or on the rock masses. It is impossible to determine the deformation modulus of rock masses in laboratory. For this reason, deformation modulus of rock mass is determined by in-situ tests. However, in-situ tests are time-consuming and sophisticated testing equipments. Therefore, empirical equations for estimating the deformation modulus of rock masses have been proposed by many researchers (i.e. Bieniawski 1973, Serafim and Pereira 1983, Nicholson and Bieniawski 1990, Grimstad and Barton 1993, Mitri *et al.* 1994, Hoek and Brown 1997, Verman *et al.* 1997, Read *et al.* 1999, Palmstrom 2000, Barton 2002, Kayabasi *et al.* 2003, Gokceoglu *et al.* 2003, Zhang and Einstein 2004, Ramamurthy 2004, Galera *et al.* 2005, Sonmez *et al.* 2004, 2006, Hoek and Diederichs 2006, Chun *et al.* 2006, Isik *et al.* 2008, Mohammadi and Rahmannejad 2010, Beiki *et al.* 2010, Ghamgosar *et al.* 2010, Shen *et al.* 2012, Martins and Miranda 2012, Alemdag *et al.* 2015, 2016). These equations have been widely used in engineering projects. However, although it has been emphasised by various researchers (Verman *et al.* 1997, Barton 2002, Martins and Miranda 2012) that the depth, in other words, the overburden load or vertical stress, has an effect on the deformation modulus. However, no research, except few studies (Verman *et al.* 1997, Martins and Miranda 2012), has been performed using the database with a large amount of data. However, recently Tokgozoglu (2021) has prepared a database including the depths in which the in-situ tests were performed. As a result of the analysis of these data, Tokgozoglu and Gokceoglu (2021) have proposed empirical relationships in which vertical stress takes place as a parameter by revealing the effect of vertical stress on deformation modulus of rock mass.

In addition to empirical equations, various artificial intelligence and soft-computing algorithms (Kayabasi *et al.* 2003, Gokceoglu *et al.* 2004, Majdi and Beiki 2010, Beiki *et al.* 2010, Bashari *et al.* 2011, Martins and Miranda 2012, Gholamnejad *et al.* 2013, Nejati *et al.* 2014, Asrari *et al.* 2015, Feng and Jimenez 2015, Asadizadeh and Hossaini 2016, Fattahi 2016) have been considered to predict deformation modulus of rock mass. A general assessment on these algorithms was carried out by Gokceoglu (2017). Among these, only the model developed by Martins and Miranda (2012) considered depth or overburden load. For this reason, the purposes of the present study are to predict

CONTACT C. Gokceoglu cgokce@hacettepe.edu.tr

deformation modulus of rock masses and to assess the effect of vertical stress employing artificial neural networ (ANN) models. In accordance with the purpose of the study, the database prepared by Tokgozoglu (2021) including deformation modulus of rock mass, intact rock and rock mass properties as well as depth is employed. The main originality of this study is that it is one of the pioneer studies in geomechanics literature to show the effect of the overburden stress on the deformation modulus of rock masses using a relatively large dataset and ANN.

Data employed

The data used in this study were compiled by Tokgozoglu (2021). The main sources of the data are the projects carried out by the Istanbul Metropolitan Municipality and the General Directorate of Infrastructure Investments in four different regions of Istanbul, Turkey (Tokgozoglu and Gokceoglu 2021). The rock types included by the database are limestone, sandstone, siltstone, claystone and shale. A total of 124 geotechnical boreholes and in-situ tests performed in these boreholes were used in the database (Tokgozoglu 2021). Discontinuity parameters were determined for RMR classification in the zones where pressuremeter tests were performed, and intact rock samples were obtained for the tests on intact rock such as uniaxial compressive strength, modulus of elasticity and unit weight by Tokgozoglu (2021).

The database used in the study consists of seven variables. Univariate descriptive statistics of all variables are presented in Table 1. In Table 1, number of observations (N), Min–Max values, Mean, Median, Mod, Range, Standard Deviation and Variance values for each variable are shown.

ANN modelling

Machine learning, which is the most popular approach of today, is based on the effective use of traditional statistical models. Machine learning and statistical methods have proved their success in analysing data in various real-world applications (Aladag 2019). Especially in recent years, the machine-learning approach has been used successfully in many studies (i.e. Yagiz *et al.* 2009, 2012, Gokceoglu *et al.* 2009, Aladag *et al.* 2013, Sevgen *et al.* 2019, Acitas *et al.* 2019, Yilmazer and Kocaman 2020). ANNs method is the heart of machine learning. Unlike traditional statistical methods, the ANN method is not satisfactory in explaining causal relationships between variables. This drawback of the method is called as black box. On the other hand, the ANN approach is a very effective prediction tool (Gundogdu *et al.* 2016). The ANN method can produce very accurate results, especially when point estimation is performed. Therefore, ANN approach has been widely used in various real-world applications and very accurate prediction results have been obtained (Aladag 2017).

In this study, the ANN method is utilised to get accurate E_m (deformation modulus of rock masses) predictions. Feed forward ANNs are employed for this prediction application. Also, different prediction models are generated in the implementation to evaluate overburden stress variable effect on E_m prediction. Therefore, modelling part of the implementation of this study is divided into two phases. In the first phase, two prediction models are not including overburden stress variable are utilised to obtain predictions for E_m. These Models 1 and 2 are presented below.

Model 1: Inputs are RMR, E_i; and Output is E_m

Model 2: Inputs are RQD, UCS, WeatDeg, Ei; and Output is E_m

In Model 1, E_m is explained by RMR and E_i values. Model 2 says that E_m caused by RQD, UCS, WeatDeg, and E_i. Therefore, for Models 1 and 2, 2 and 4 neurons are, respectively, used in the input layers of ANN architectures. For each hidden layer, the number of neurons are changed from 1 to 20 in constructing the architectures of ANN. The data are divided into two sets namely training and test sets. ANN models are trained by utilising training set. Then, the prediction performances are evaluated over the test set. Backpropagation algorithm is

Table 1. The descriptive statistics of the data (E_m: deformation modulus of rock mass; RQD: rock quality designation; UCS: uniaxial compressive strength; WeatDeg: weathering degree; E_i: elasticity modulus of intact rock; σ_v: overburden stress).

	E_m (MPa)	RQD (%)	UCS (MPa)	RMR	WeatDeg	E_i (GPa)	σ_v (t/m^2)
N	329	2406	747	2427	2398	711	2441
Min	1.16	0	0.60	21	1	0	1.32
Max	7273.40	100	134.60	69	6	37.90	267.72
Mean	1472.00	55.83	31.13	40.17	3.05	10.77	71.60
Median	912	60	26.80	40	3	9.10	66.69
Mod	403.40	100	15.50	53	3	0.40	70.74
Range	7272.24	100	134	48	5	37.90	266.40
Standard Deviation	1527.21	37.64	23.08	11.28	0.81	8.75	39.74
Variance	2332378.83	1416.56	532.68	127.21	0.66	76.64	1579.03

used as training algorithm. It is a well-known fact that ANN approach is very good in modelling both nonlinear and linear structures by activation function (Egrioglu *et al.* 2015). In this study, in all neurons of the hidden layer, tangent sigmoid activation function, which is a nonlinear function, is used. Purelin linear activation function is utilised in the output neuron. Therefore, nonlinear and linear structures in the data can be modelled by ANN models. There are various activation functions used in the literature. Tangent sigmoid is used in this study since it is one of the most used functions in the literature (Gundogdu *et al.* 2016).

For Model 1, total 141 cases are employed. While 126 observations are used for training, the rest 15 observations are used for the test set. All examined ANN architectures have two input neurons corresponding to RMR and E_i variables in Model 1 while one output neuron is for E_m variable. The number of neurons in hidden layer is changed from 1 to 20. Thus, 20 architectures are examined for Model 1. All obtained prediction results obtained prediction results for the test data are presented in Table 2. In this table, NHL (neurons in hidden layer), VAF (values account for) and RMSE (root mean square error). 20 ANN architectures are ordered in Table 2 from the best to the worst according to their RMSE values.

Table 2. Prediction results obtained from ANN architectures for the Model 1.

NHL	VAF (%)	RMSE	NHL	VAF (%)	RMSE
17	73.33	462.3660	6	17.28	1134.1152
20	72.67	493.5400	3	12.43	1135.2147
11	60.22	703.2752	14	48.54	1139.6497
16	64.00	783.5336	12	52.12	1189.5906
18	65.41	921.2585	2	13.32	1249.0419
19	67.91	937.1108	5	15.57	1262.1203
9	45.71	1019.2331	15	62.99	1271.2772
13	58.80	1081.5898	4	23.68	1289.4913
8	34.97	1093.0825	1	11.19	1295.9155
7	34.37	1097.4140	10	38.15	1316.2348

According to Table 2, it is seen that the best RMSE value is obtained when ANN architecture includes 17 neurons in hidden layer is used. Since Model 1 is applied and just one output neuron is utilised in all architectures, the best architecture (2–17-1) has 1, 16 and 2 neurons in output, hidden, and input layers, respectively. This architecture has the best RMSE values 462.3660. Also, 2–17-1 architecture has VAF value 73.33%, which shows this architecture gives good predictions. In order to show the training performance of the determined model 2–17-1, cross-correlation graph is given in Figure 1. This graph shows that this ANN architecture is trained well.

Table 3 is given to examine the prediction performance of 2–17-1 ANN model. In Table 3, for the test set, the observed and the predicted values obtained from 2–17-1 ANN model are presented. When Table 3 is examined, it is clearly seen that the fitness between the

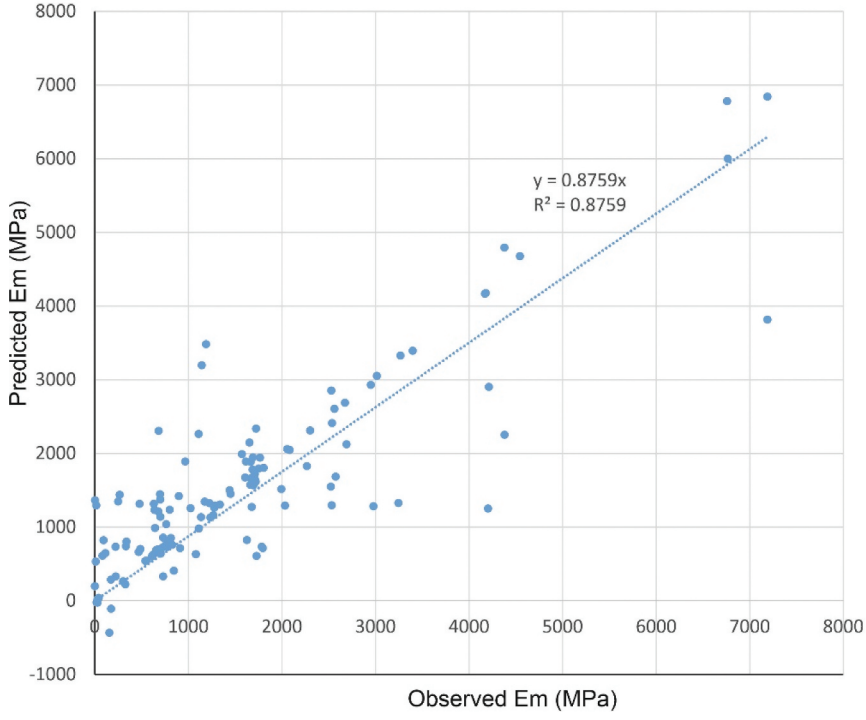

Figure 1. Cross-correlation graph of training dataset for the Model 1.

Table 3. The observed and the predicted values obtained from 2–17-1 for the test set.

Observation No	Observed	Predicted	Observation No	Observed	Predicted
1	42.27	345.9270	9	1573.40	1529.1004
2	225.40	350.9236	10	1673.60	1612.0591
3	477.90	204.7900	11	1720.10	1901.7151
4	645.30	621.5020	12	1994.90	1948.4668
5	700.90	1146.0357	13	2531.70	2553.0459
6	779.70	733.8172	14	3015.40	3016.4398
7	1024.00	1586.6973	15	4377.90	4216.7208
8	1226.70	1768.5449			

observations and the predictions are good. That is, 2–17-1ANN model produces satisfactory predictions for the test set includes 15 observations.

Also, the prediction results of the best architecture are examined visually. In Figure 2, the observed and the predicted values obtained from 2–17-1 are presented. In Figure 2, vertical and horizontal axes show E_m values and observation numbers, respectively. When this graph is examined, it can be said that the fitness between the observations and the predictions is good. Also, the goodness of the predictions obtained for the test set also indicates that there is no overfitting problem.

For Model 2, there are 135 observations recorded. While 120 observations are being used for training, the rest 15 observations are being used for the test set. All examined ANN architectures have four input neurons corresponding to RQD, UCS, Weathering Degree and E_i variables in Model 2 while one output neuron is for E_m variable. The number of neurons in hidden layer is changed from 1 to 20. Thus, 20 architectures are examined for Model 2. All obtained prediction results are presented in Table 4. In this table, NHL, VAF and RMSE, respectively, represents the number of neurons in hidden layer, variance percentage, and root-mean-square error values calculated over the test set. All examined ANN architectures are ordered in the table from the best to the worst in terms of RMSE values.

According to Table 4, it is seen that the best RMSE value is produced by 4–17-1 ANN architecture. The best architecture 4–17-1 has 1, 17 and 4 neurons in output, hidden, and input layers, respectively. This architecture has the best RMSE values 109,4394. Also, it has VAF value 94,13%. Therefore, it can be said that this architecture gives accurate predictions in terms of RMSE and VAF measures. In order to show the training performance of the determined model 4–17-1, cross-correlation graph is given in Figure 3. According to this graph, it is clear that this ANN architecture is trained considerably.

Table 5 shows the results of the prediction performance of 4–17-1 ANN model. In Table 5, for the test set, the observed and the predicted values obtained from 4–

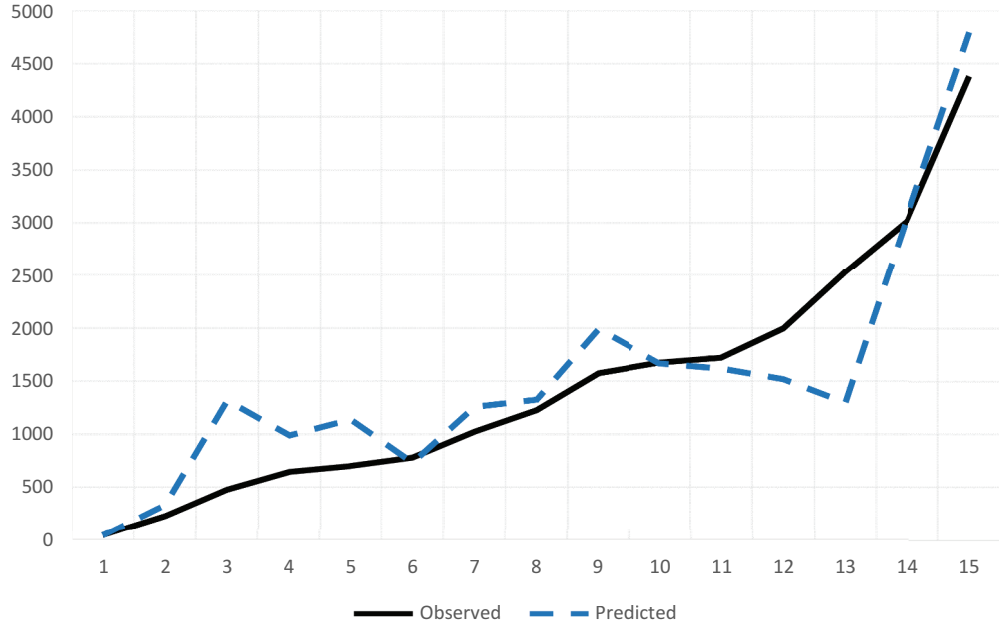

Figure 2. The observations and the predictions obtained from 2–17-1 structured ANN model.

Table 4. Prediction results obtained from ANN architectures for Model 2.

NHL	VAF (%)	RMSE	NHL	VAF (%)	RMSE
17	94,13	109,4394	10	75,38	798,4387
20	96,20	112,7578	8	73,47	885,3361
19	96,83	115,0254	7	47,74	1118,6098
18	97,70	233,0153	4	41,74	1303,9469
14	92,77	235,3550	9	63,04	1310,6134
16	95,64	247,0734	6	45,13	1318,1165
15	92,37	350,7074	5	45,35	1330,0361
12	89,91	367,6450	3	28,06	1679,0978
13	83,84	570,4796	1	15,76	1728,3505
11	73,65	769,6805	2	24,25	1764,0905

17-1 ANN model are given. From Table 5, it is clearly seen that the observations and the predictions are close. That is, 4–17-1 ANN model produces satisfactory predictions.

To evaluate the prediction performance of the best ANN architecture for Model 2 better, the graph of the observations and the predictions produced by the best architecture is given in Figure 4. According to the graph given in Figure 4, it is observed that the fitness between the observations and the predictions is satisfactory. Also, the goodness of the predictions obtained for the test set also indicates that there is no overfitting problem. When comparing Models 1 and 2, it is clearly seen that the results obtained for Model 2 are much better. Therefore, in order to reach high prediction accuracy, it would be wise to use RQD, UCS, and Weathering Degree variables instead of using RMR variable when Overburden stress variable is not included in prediction models.

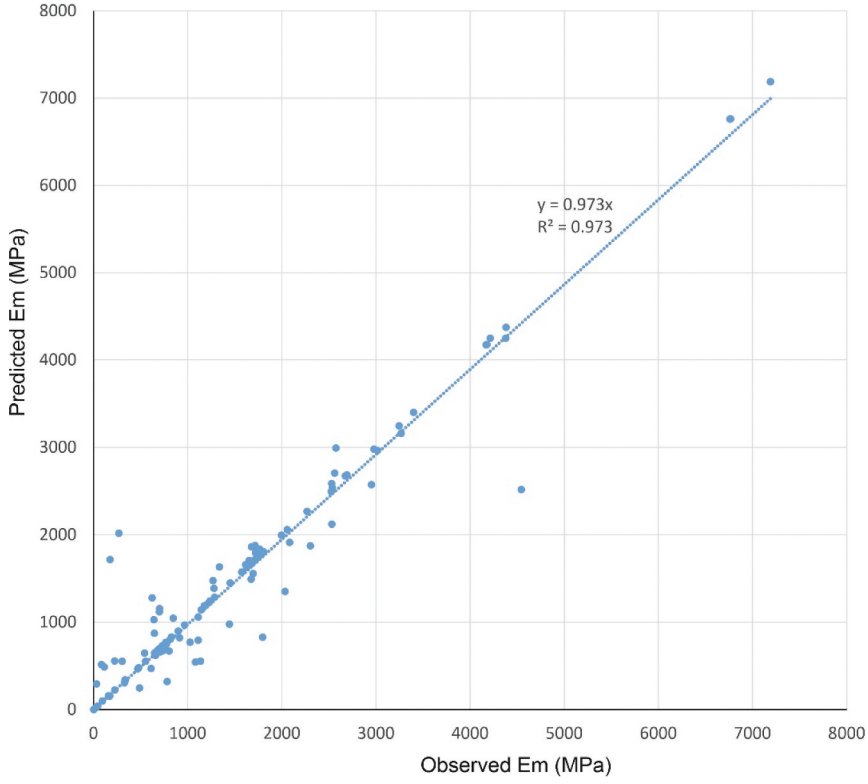

Figure 3. Cross-correlation graph of training dataset for the Model 2.

Table 5. The observed and the predicted values obtained from 4–17-1 for the test set.

Observation No	Observed	Predicted	Observation No	Observed	Predicted
1	42.27	42.1650	9	1653.10	1705.1121
2	225.40	225.3833	10	1690.90	1691.8547
3	488.30	246.4562	11	1766.30	1833.4913
4	657.20	619.7550	12	2267.70	2267.7281
5	730.50	730.3700	13	2674.20	2674.1703
6	827.20	830.6395	14	4170.00	4173.1734
7	1111.50	794.2291	15	7188.90	7189.0013
8	1279.10	1388.0068			

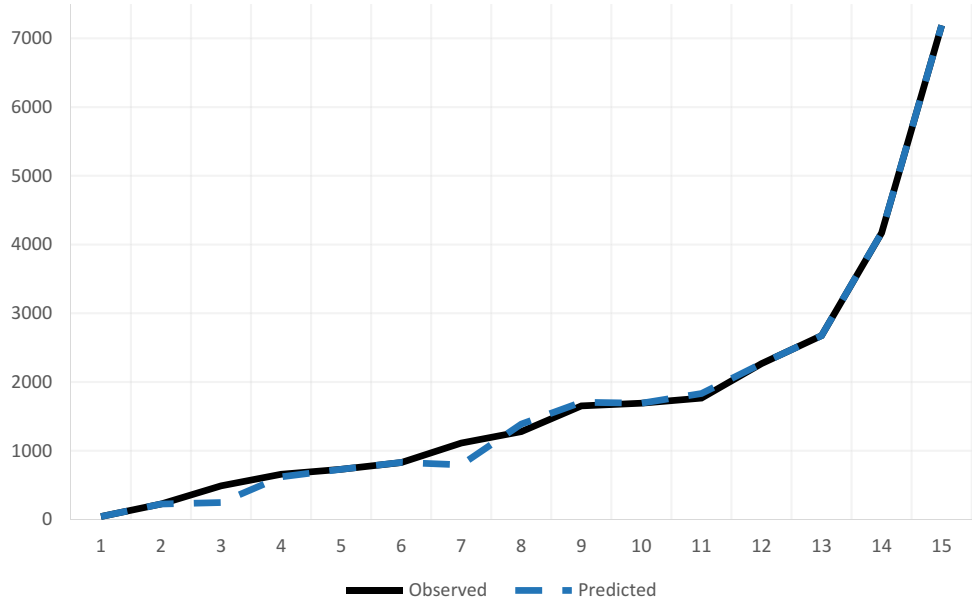

Figure 4. The observations and the predictions obtained from 4–17-1.

In the second part of the implementation, two different prediction models are generated by adding Overburden stress variable. These predictions models are given below.

Model 3: RMR, Overburden stress, $E_i \longrightarrow E_m$

Model 4: RQD, UCS, Weathering Degree, Overburden stress, $E_i \longrightarrow E_m$

According to Model 3, E_m is explained by RMR, Overburden stress, and E_i values. Model 2 shows that E_m caused by RQD, UCS, Weathering Degree, Overburden stress, and E_i. Therefore, for Models 3 and 4, 3 and 5 neurons are, respectively, used in the input layers of ANN architectures.

For Model 3, total 141 cases are utilised. While 126 observations are used for training, the rest 15 observations are used for the test set. Three input neurons are employed since RMR, Overburden stress, and E_i are independent variables in Model 3. The number of neurons in hidden layer are changed from 1 to 20, and one output neuron corresponding E_m variable is used for all architectures. Thus, 20 architectures are examined for Model 3. All obtained prediction results are presented in Table 6. In Table 6, NHL, VAF and RMSE, respectively, represents the number of neurons in hidden layer, variance percentage, and root-mean-square error values calculated over the test set. 20 ANN architectures are ordered in the table from the best to the worst according to their RMSE values.

In Table 6, it is seen that the best RMSE value is obtained when ANN architecture includes 16 neurons in hidden layer is employed. Since Model 3 is applied and just one output neuron is utilised in all architectures, the best architecture (3–16-1) has 1, 16 and 3 neurons in output, hidden, and input layers, respectively. This architecture has the best RMSE values 265.9473. Also, 3–16-1 architecture produces 100% VAF value, which shows this architecture gives good predictions. In order to show the training performance of the determined model 3–16-1, cross-correlation graph is presented in Figure 5. According to this graph, it is observed that this ANN architecture is trained well.

Table 6. Prediction results obtained from one hidden-layered architectures for Model 3.

NNHL	VAF (%)	RMSE	NNHL	VAF (%)	RMSE
16	90.57	265.9473	8	54.94	1015.9695
20	96.51	290.6045	14	67.57	1087.3136
19	94.77	380.6939	1	14.65	1135.6559
15	85.87	474.2680	6	54.73	1160.5461
12	81.75	656.7960	2	16.71	1172.0397
18	92.26	679.0235	3	27.38	1187.5709
13	78.70	802.1813	10	63.92	1219.3061
17	82.31	837.0672	5	38.86	1276.1568
11	78.48	1000.0813	4	36.57	1290.0094
9	66.96	1013.0875	7	47.77	1296.1241

Table 7 is given to show the prediction performance of 4–17-1 ANN model. In Table 7, for the test set, the observed and the predicted values obtained from 3–16-1 ANN model are given. When Table 7 is examined, it is observed that 3–16-1 ANN model gives satisfying results.

The predictions obtained from the best architecture 3–16-1 are also examined visually. For this purpose, the graph of the observations and the predictions produced by 3–16-1 architecture is presented in Figure 6. In Figure 6, vertical and horizontal axes represent E_m

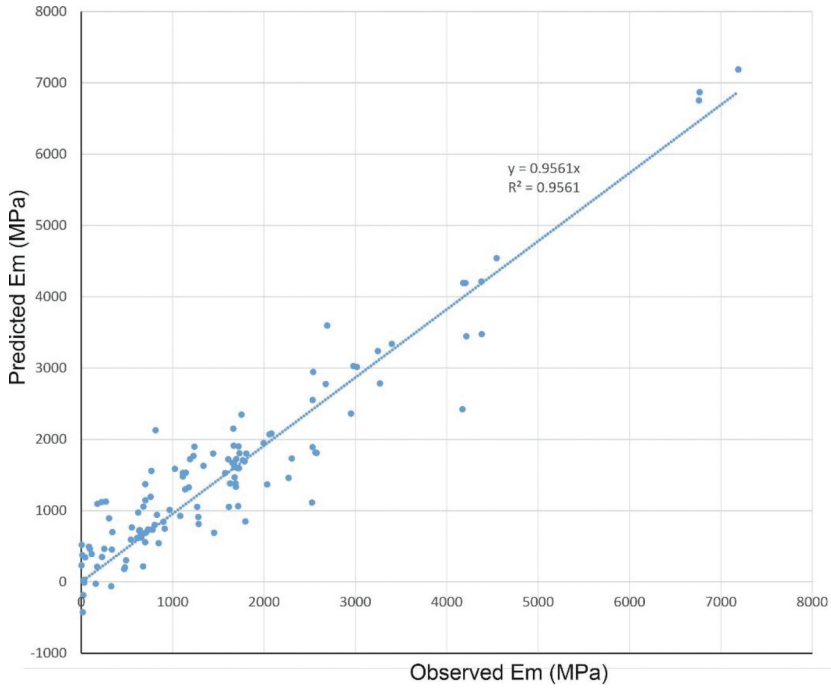

Figure 5. Cross-correlation graph of training dataset for the Model 3.

Table 7. The observed and the predicted values obtained from 3–16-1 for the test set.

Observation No	Observed	Predicted	Observation No	Observed	Predicted
1	42.27	345.9270	9	1573.40	1529.1004
2	225.40	350.9236	10	1673.60	1612.0591
3	477.90	204.7900	11	1720.10	1901.7151
4	645.30	621.5020	12	1994.90	1948.4668
5	700.90	1146.0357	13	2531.70	2553.0459
6	779.70	733.8172	14	3015.40	3016.4398
7	1024.00	1586.6973	15	4377.90	4216.7208
8	1226.70	1768.5449			

values and observation numbers, respectively. From Figure 6, it is can be said that the observations and the corresponding predictions are very close. This is, 3–16-1 model gives accurate results. Also, the goodness of the predictions obtained for the test set also indicates that there is no overfitting problem.

For Model 4, total 135 cases are included. While 120 observations are being used for training, the rest 15 observations are being used for the test set. In this case, there are five input neurons for RQD, UCS, Weathering Degree, Overburden stress, and E_i independent variables in Model 4. The number of neurons in hidden layer are changed from 1 to 20, and one output neuron corresponding E_m variable is used for all architectures. Therefore, 20 architectures are examined for Model 4. All obtained prediction results are presented in Table 8. All examined ANN architectures are ordered in the table from the best to the worst in terms of RMSE value.

From Table 8, it is observed that the best RMSE value is obtained when 17 neurons are used in hidden layer. Since Model 4 is applied and just one output neuron is utilised, the best architecture (5–17-1) has 1, 17 and 5 neurons in output, hidden, and input layers, respectively. This architecture gives the best RMSE value 17.7337 and, 3–16-1 architecture has 99.97% VAF value. Therefore, it can be said that 5–17-1 model produces very accurate predictions. In order to show the training performance of the determined model 5–17-1, cross-correlation graph is presented in Figure 5. According to this graph, it is clearly seen that this ANN architecture is trained exceptionally.

Table 9 is given to show the prediction performance of 5–17-1 ANN model. This table presents the observed and the predicted values obtained from 5–17-1 ANN model for the test set. According to Table 9, it is clearly seen that 5–17-1 ANN model gives accurate results.

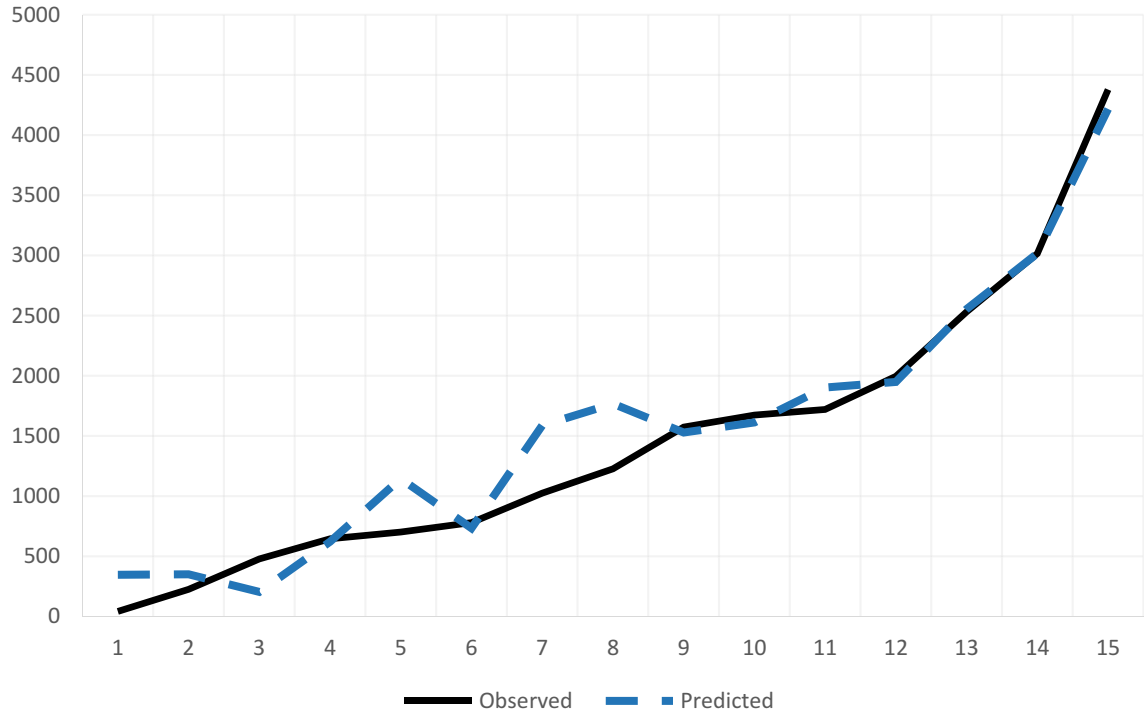

Figure 6. The observations and the predictions obtained from 3–16-1.

Table 8. Prediction results obtained from one hidden-layered architecture for Model 4.

NHL	VAF (%)	RMSE	NHL	VAF (%)	RMSE
17	99.97	17.7337	10	89.11	364.0315
19	99.98	20.5602	6	76.83	399.3151
18	99.98	21.4189	9	87.70	479.7347
20	99.97	23.7843	8	83.25	576.2689
16	99.85	58.3059	7	55.92	776.5997
15	98.49	125.9001	3	57.56	817.6682
13	95.67	224.5623	5	64.55	852.7408
14	93.23	236.4518	2	29.03	1371.1293
12	93.64	244.4570	4	16.07	1648.6191
11	85.68	250.9482	1	16.23	1706.9355

Table 9. The observed and the predicted values obtained from 5–17-1 for the test set.

Observation No	Observed	Predicted	Observation No	Observed	Predicted
1	42.27	42.7760	9	1653.10	1649.4215
2	225.40	221.2784	10	1690.90	1695.0723
3	488.30	488.3825	11	1766.30	1712.8505
4	657.20	679.9772	12	2267.70	2273.8461
5	730.50	733.2810	13	2674.20	2672.4598
6	827.20	827.1301	14	4170.00	4177.7667
7	1111.50	1125.5286	15	7188.90	7220.2433
8	1279.10	1281.4166			

In order to evaluate the performance of 5–17-1 ANN model, the predictions are also examined by visually. For the purpose of this aim, the graph of the observations and the predictions produced by 5–17-1 is shown in Figure 8. According to Figure 8,Figure 7 it is clearly observed that the fitness between the observations and the predictions is perfect. 5–17-1 ANN model gives very accurate predictions. Also, the goodness of the predictions obtained for the test set also indicates that there is no overfitting problem.

Results and discussion

For each prediction models, 20 feed-forward neural network architectures are examined in all applications. 80 different architectures in total are applied to the data. All prediction results obtained from the best architectures are summarised in Table 10.

As seen from Table 10, it is clearly seen that as the number of inputs increases, better predictions are obtained in terms of RMSE and VAF measures. Statistically speaking, this is an expected result since as the number of independent variables increases, the dependent variable is expected to be better predicted. According to Table 10, the worst estimation results are obtained when Model 1 is used in terms of both RMSE and VAF criteria. The most accurate predictions are obtained when Model 4 is employed. 5–17-1 ANN architecture for Model 4 produces accurate predictions. Here, Model 1 and Model 3, Model 2 and Model 4 should be compared because Model 3 is the version of Model 1 containing Overburden stress parameter. In addition, Model 4 is the version of Model 2 that contains Overburden stress parameter. All obtained prediction results summarised in Table 10 can be examined to evaluate the significance of Overburden stress variable

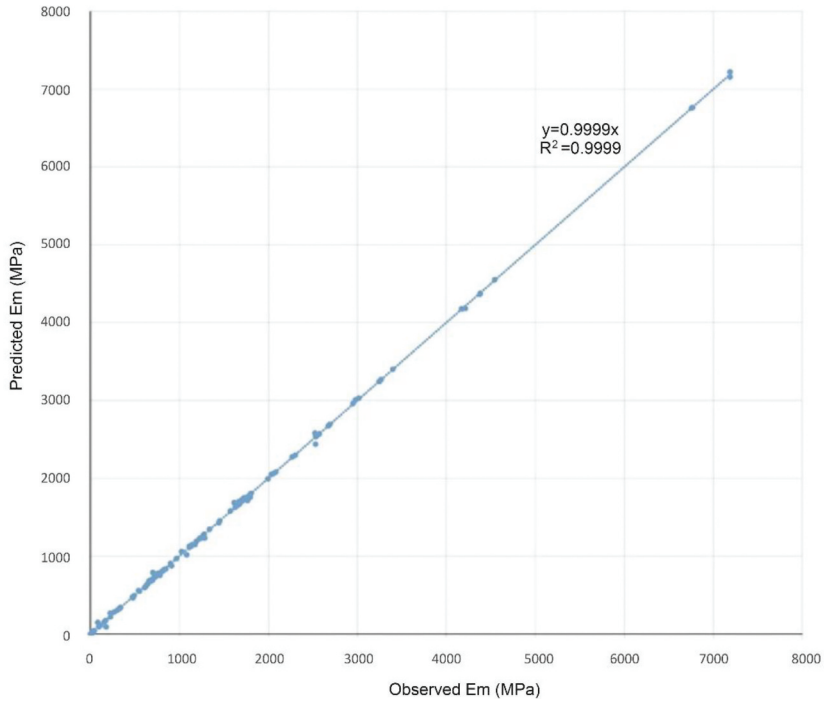

Figure 7. Cross-correlation graph of training dataset for the Model 2.

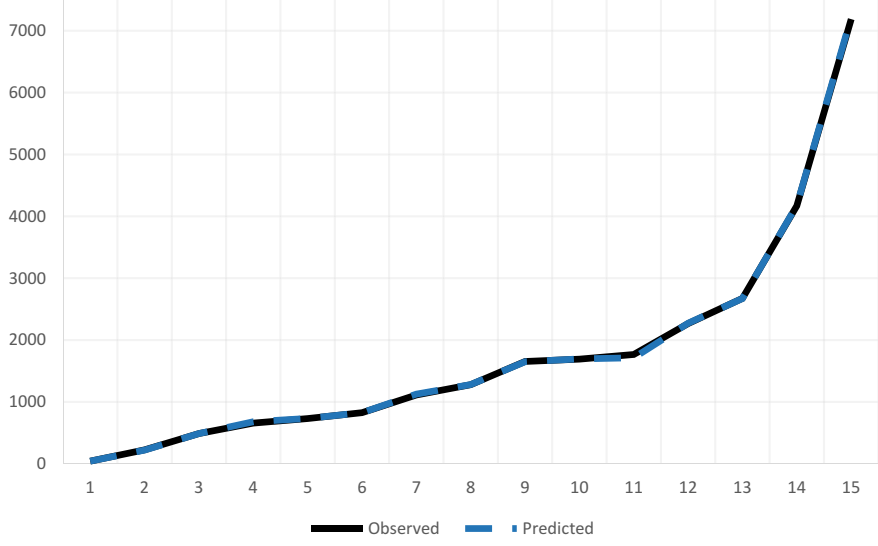

Figure 8. The observations and the predictions obtained from 5–17-1.

Table 10. All obtained prediction results.

	The Best Architecture	VAF (%)	RMSE
Model 1	2–17-1	73.33	462.3660
Model 2	4–17-1	94.13	109.4394
Model 3	3–16-1	90.57	265.9473
Model 4	5–17-1	99.97	17.7337

on explaining E_m. When Model 1 (RMR, $E_i \longrightarrow E_m$) and Model 3 (RMR, E_i, Overburden stress $\longrightarrow E_m$) is compared, it is clearly seen that the prediction accuracy is increased by using Overburden stress variable. In a similar way, if Model 2 (RQD, UCS, Weathering Degree, Ei $\longrightarrow E_m$) and Model 4 (RQD, UCS, Weathering Degree, E_i, Overburden stress $\longrightarrow E_m$) is compared, it is clearly observed that the prediction accuracy is increased considerably by adding Overburden stress to the prediction model. Therefore, it can be clearly said that Overburden

stress is an important variable to predict E_m accurately. Consequently, the most accurate prediction results are obtained when the prediction model includes Overburden stress variable.

Models 1 and 3 produced some negative E_m values (refer Figures 1 and 5). However, such a problem was not observed in Models 2 and 4 (see Figures 3 and 7). The main reason for this problem is thought to be the input parameters. When E_i and weathering degree are included in the models, it is seen that the negative value problem is eliminated. Therefore, it can be said that E_i and weathering degree should be taken into account in the models to be developed for the prediction of E_m.

Verman *et al.* (1997) proposed the following equation to calculate the deformation modulus of a rock mass around an underground opening at a certain depth:

$$E = 0.3H^{\alpha}10(RMR - 20)/38$$

The equation proposed by Verman *et al.* (1997) for the rock mass deformation modulus considers depth, and 'α' is a coefficient varying between 0.16 and 0.30. Despite its limitations, the equation of Verman *et al.* (1997) is extremely important, as it is the first deformation modulus equation in the literature that considers depth. The effect of depth on Q has also been studied by Barton (2002). In the Gjovik Underground Space Region (Norway), it has been observed that the compressional wave velocity (V_p) continuously increases with depth, although the rock quality designation (RQD) and the number of joints per metre are almost constant in the depth range of 0–70 m (Barton 2002). Martins and Miranda (2012) suggested some prediction models of the deformation modulus of a rock mass, and their results showed that one of the most important parameters governing the deformation modulus is depth. Verman *et al.* (1997) stated that the deformation modulus of a rock mass increases with the RMR and tunnel depth. In the present study, the similar results have been obtained, however the database used in the study refers to a depth range of 5.00–120 metres. In other words, the database represents relatively shallow depth. The main reason of this increase in E_m may be crack closure.

In the implementation part, the best ANN architectures for each four models are given. Parameters of these ANN models, which is weight values, are given in Appendix A in order to use these models in further studies.

Conclusions

The conclusions obtained from the study can be summarised as follows:

In all data-driven approaches, the number and quality of the data used in the model development stage are important. In this study, the database prepared by Tokgozoglu (2021) was used. This database includes both in-situ pressiometer test results, as well as whole rock mass and intact rock parameters. While developing the models, attention has been paid to using the parameters considered in standard rock engineering studies.

Modelling studies are basically considered as two stages. In the first stage, Model 1 (RMR, $E_i \longrightarrow E_m$) and Model 2 (RQD, UCS, Weathering Degree, $Ei \longrightarrow E_m$) were constructed. VAF indices of Model 1 and Model 2 were obtained as 73.33 and 94.13, respectively. Model 3 and Model 4 are extremely important in understanding the effect of Overburden stress on E_m. Adding the Overburden stress parameter to Model 1 and Model 2 increases the VAF index of Model 3 to 90.57, and the VAF index of Model 4 to 99.97%. These results clearly demonstrated the effect of overburden stress on E_m. Results of the present study suggest that overburden stress should be considered in order to predict the rock mass, accurately. In addition, model weights are presented as an Appendix A for practical use in engineering applications.

Accurate prediction of rock mass deformation modulus will allow the development of safer and optimum projects, especially for rock engineering structures to be constructed at certain depths from the surface. However, like any data-driven study, the results of this study should be checked before being used directly in projects. In addition, the models developed in the present study are valid for sedimentary rocks and shallow depths (50–120 metres).

Disclosure statement

No potential conflict of interest was reported by the author(s).

ORCID

K. Tokgozoglu http://orcid.org/0000-0001-8872-8212

References

Acitas, S., Aladag, C.H., and Senoglu, B., 2019. A new approach for estimating the parameters of Weibull distribution via particle swarm optimization: an application to the strengths of glass fiber data. *Reliability Engineering and System Safety*, 183, 116–127. doi:10.1016/j.ress.2018.07.024

Aladag, C.H., ed., 2017. *Advances in time series forecasting*. Vol. 2. Sharjah, U.A.E: Bentham Science Publishers Ltd.

Aladag, C.H., 2019. Architecture selection in neural networks by statistical and machine learning. *Oriental Journal of Computer Science and Technology*, 12 (3), 76–89. doi:10.13005/ojcst12.03.02.

Aladag, C.H., Kayabasi, A., and Gokceoglu, C., 2013. Estimation of pressuremeter modulus and limit pressure of clayey soils by various artificial neural network models. *Neural Computing & Applications*, 23 (2), 333–339. doi:10.1007/s00521-012-0900-y.

Alemdag, S., *et al*., 2016. Modeling deformation modulus of a stratified sedimentary rock mass using neural network, fuzzy inference and genetic programming. *Engineering Geology*, 203, 70–82. doi:10.1016/j.enggeo.2015.12.002

Alemdag, S., Gurocak, Z., and Gokceoglu, C., 2015. A simple regression-based approach to estimate deformation modulus of rock masses. *Journal of African Earth Sciences*, 110, 75–80. doi:10.1016/j.jafrearsci.2015.06.011

Asadizadeh, M. and Hossaini, M.F., 2016. Predicting rock mass deformation modulus by artificial intelligence approach based on dilatometer tests. *Arabian Journal of Geosciences*, 9 (2), Article No 96. doi:10.1007/s12517-015-2189-5.

Asrari, A.A., Shahriar, K., and Ataeepour, M., 2015. The performance of ANFIS model for prediction of deformation modulus of rock mass. *Arabian Journal of Geosciences*, 8 (1), 357–365. doi:10.1007/s12517-013-1097-9.

Barton, N., 2002. Some new Q-Value correlations to assist in rock masses for design of tunnel design. *International Journal of Rock Mechanics and Mining Sciences*, 39 (2), 185–216. doi:10.1016/S1365-1609(02)00011-4.

Bashari, A., Beiki, M., and Talebinejad, A., 2011. Estimation of deformation modulus of rock masses by using fuzzy clustering-based modelling. *International Journal of Rock Mechanics and Mining Sciences*, 48, 1224–1234. doi:10.1016/j.ijrmms.2011.09.017

Beiki, M., Bashari, A., and Majdi, A., 2010. Genetic programming approach for estimating the deformation modulus of rock mass using sensitivity analysis by neural network. *International Journal of Rock Mechanics and Mining Sciences*, 47, 1091–1103. doi:10.1016/j.ijrmms.2010.07.007

Bieniawski, Z.T., 1973. Engineering classification of rock masses. *Transactions South African Institution of Civil Engineers*, 15, 335–344.

Chun, B., *et al*., 2006. Correlation of deformation modulus by PMT with RMR and rock mass condition. *Tunnelling and Underground Space Technology*, 21 (3–4), 231–232. doi:10.1016/j.tust.2005.12.011.

Egrioglu, E., *et al*., 2015. Recurrent multiplicative neuron model artificial neural network for non-linear time series forecasting. *Neural Processing Letters*, 41 (2), 249–258. doi:10.1007/s11063-014-9342-0.

Fattahi, H., 2016. Indirect estimation of deformation modulus of an in situ rock mass: an ANFIS model based on grid partitioning, fuzzy c-means clustering and subtractive clustering. *Geosciences Journal*, 20 (5), 681–690. doi:10.1007/s12303-015-0065-7.

Feng, X. and Jimenez, R., 2015. Estimation of deformation modulus of rock masses based on Bayesian model selection and Bayesian updating approach. *Engineering Geology*, 199, 19–27. doi:10.1016/j.enggeo.2015.10.002

Galera, J.M., Alvarez, Z., and Bieniawski, Z.T., 2005. Evaluation of the deformation modulus of rock masses: comparison between pressure meter and dilatometer tests with RMR predictions. *In*: Proceedings ISP5-PRESSIO 2005 Paris, France. Gambin, Magnen, Mestat, and Baguelin, eds. LCPC Publication Paris.

Ghamgosar, M., Fahimifar, A., and Rasouli, V., 2010. Estimation of rock mass deformation modulus from laboratory experiments in Karun dam. *In*: *Proceedings of the International Symposium of the International Society for Rock Mechanics*. Zhao, Laboise, Dudt and Mathier, eds. Taylor & Francis Group, 805–808.

Gholamnejad, J., Bahaaddini, H., and Rastegar, M., 2013. Prediction of the deformation modulus of rock masses using artificial neural networks and regression methods. *Journal of Mining and Environment*, 4 (1), 35–43.

Gokceoglu, C., *et al*., 2009. A comparative study on indirect determination of degree of weathering of granites from some physical and strength parameters by two soft computing techniques. *Materials Characterization*, 60 (11), 1317–1327. doi:10.1016/j.matchar.2009.06.006.

Gokceoglu, C., 2017. Deformation modulus (Em) of rock masses: recent developments. Proceedings of the ISRM 3rd Nordic Rock Mechanics Symposium - NRMS 2017, Helsinki, Finland, October. ISRM-NRMS-2017-003.

Gokceoglu, C., Sonmez, H., and Kayabasi, A., 2003. Prediction the deformation moduli of rock masses. *International Journal of Rock Mechanics and Mining Sciences*, 40, 703–712. doi:10.1016/S1365-1609(03)00062-5

Gokceoglu, C., Yesilnacar, E., Sonmez, H., & Kayabasi, A. (2004). A neuro-fuzzy model for modulus of deformation of jointed rock masses. Computers and Geotechnics, 31(5), 375–383.

Grimstad, E. and Barton, N., 1993. Updating the Q-System for NMT. *In*: *Proceedings of the International Symposium on Sprayed Concrete-Modern Use of Wet Mix Sprayed Concrete for underground Support*. Oslo: Norwegian Concrete Association.

Gundogdu, O., *et al*., 2016. Multiplicative neuron model artificial neural network based on Gaussian activation function. *Neural Computing & Applications*, 27 (4), 927–935. doi:10.1007/s00521-015-1908-x.

Hoek, E. and Brown, E.T., 1997. Practical estimates of rock mass strength. *International Journal of Rock Mechanics and Mining Sciences*, 34 (8), 1165–1186. doi:10.1016/S1365-1609(97)80069-X.

Hoek, E. and Diederichs, M., 2006. Empirical estimation of rock mass modulus. *International Journal of Rock Mechanics and Mining Sciences*, 43, 203–215. doi:10.1016/j.ijrmms.2005.06.005

Isik, N.S., Ulusay, R., and Doyuran, V., 2008. Deformation modulus of heavily jointed-sheared and blocky greywackes by pressuremeter tests: numerical, experimental and empirical assessments. *Engineering Geology*, 101, 269–282. doi:10.1016/j.enggeo.2008.06.004

Kayabasi, A., Gokceoglu, C., and Ercanoglu, M., 2003. Estimating the deformation modulus rock masses: a comparative study. *International Journal of Rock Mechanics and Mining Sciences*, 40, 55–63. doi:10.1016/S1365-1609(02)00112-0

Majdi, A. and Beiki, M., 2010. Evolving neural network using a genetic algorithm for predicting the deformation modulus of rock masses. *International Journal of Rock Mechanics and Mining Sciences*, 47 (2), 246–253. doi:10.1016/j.ijrmms.2009.09.011.

Martins, F.F. and Miranda, T.F.S., 2012. Estimation of the rock deformation modulus and RMR based on data mining techniques. *Geotechnical and Geological Engineering*, 30, 787–801. doi:10.1007/s10706-012-9498-1

Mitri, H.S., Edrissi, R., and Henning, J., 1994. Finite element modeling of cable bolted stopes in hard rock ground mines. *In*: *Presented at the SME annual meeting*. New Mexico, Albuquerque, 94–116.

Mohammadi, H. and Rahmannejad, R., 2010. The estimation of deformation modulus using regression and artificial neural network analysis. *The Arabian Journal for Science and Engineering*, 35, 205–217.

Nejati, H.R., *et al*., 2014. On the use of the RMR system for estimation of rock mass deformation modulus. *Bulletin of Engineering Geology and the Environment*, 73, 531–540. doi:10.1007/s10064-013-0522-3

Nicholson, G.A. and Bieniawski, Z.T., 1990. A nonlinear deformation modulus based on rock mass classification. *International Journal of Mining and Geological Engineering*, 8, 181–202. doi:10.1007/BF01554041

Palmstrom, A., 2000. Recent developments in rock support estimates by the RMi. *Journal of Rock Mechanics and Tunnelling Technology*, 6 (1), 1–19.

Ramamurthy, T., 2004. A geo-engineering classification for rocks and rock masses. *International Journal of Rock Mechanics and Mining Sciences*, 41, 89–101. doi:10.1016/S1365-1609(03)00078-9

Read, S.A.L., Richards, L.R., and Perrin, N.D., 1999. Applicability of the Hoek–Brown failure criterion to New Zealand greywacke rocks. *In*: G. Vouille, and P. Berest (9th ISRM Congress), eds. *Proceedings of the nineth international congress on rock mechanics*. Paris, 655–660 / ISRM-9CONGRESS-1999-133. August 2.

Serafim, J.L. and Pereira, J.P., 1983. Considerations of the geomechanics considerations of Bieniawski. *In*: *Proceedings of the International Symposium on Engineering Geology and Underground Construction, LNEC*. Lisbon, Portugal, 33–42.

Sevgen, E., *et al*., 2019. A novel performance assessment approach using photogrammetric techniques for landslide susceptibility mapping with logistic regression, ANN and random forest. *Sensors*, 19 (18), 3940. doi:10.3390/s19183940.

Shen, J., Karakus, M., and Xu, C., 2012. A comparative study for empirical equation in estimating deformation modulus of rock masses. *Tunneling and Underground Space Technology*, 32, 245–250. doi:10.1016/j.tust.2012.07.004

Sonmez, H., *et al*., 2006. Estimating of rock modulus: for intact rocks with an artificial neural network and for rock masses with a new empirical equation. *International Journal of Rock Mechanics and Mining Sciences*, 43, 224–235. doi:10.1016/j.ijrmms.2005.06.007

Sonmez, H., Gokceoglu, C., and Ulusay, R., 2004. Indirect determination of the modulus of deformation of rock masses based on the GSI system. *International Journal of Rock Mechanics and Mining Sciences*, 41 (5), 849–857. doi:10.1016/j.ijrmms.2003.01.006.

Tokgozoglu, K., 2021. Investigating the effect of depth on modulus of deformation of rock masses with low strength. PhD Thesis, Hacettepe University, 190p (unpublished, in Turkish).

Tokgozoglu, K. and Gokceoglu, C., 2021. Effect of overburden stress on the deformation modulus of rock masses: an empirical study. In Review.

Verman, M., *et al*., 1997. Effect of tunnel depth on modulus of deformation of rock mass. *Rock Mechanics and Rock Engineering*, 30, 121–127. doi:10.1007/BF01047388

Yagiz, S., *et al*., 2009. Application of two non-linear prediction tools to the estimation of tunnel boring machine performance. *Engineering Applications of Artificial Intelligence*, 22 (4–5), 808–814. doi:10.1016/j.engappai.2009.03.007.

Yagiz, S., Sezer, E.A., and Gokceoglu, C., 2012. Artificial neural networks and nonlinear regression techniques to assess the influence of slake durability cycles on the prediction of uniaxial compressive strength and modulus of elasticity for carbonate rocks. *International Journal for Numerical and Analytical Methods in Geomechanics*, 36 (12), 1636–1650. doi:10.1002/nag.1066.

Yilmazer, E. and Kocaman, S., 2020. A mass appraisal assessment study using machine learning based on multiple regression and random forest. *Land Use Policy*, 99, 104889. doi:10.1016/j.landusepol.2020.104889

Zhang, L. and Einstein, H.H., 2004. Using RQD to estimate the deformation modulus of rock masses. *International Journal of Rock Mechanics and Mining Sciences*, 41, 337–341. doi:10.1016/S1365-1609(03)00100-X

Appendix A

Explanation:

$w_{ie,r}$ represents the weights between e th input neuron and r th hidden neuron. w_{he} represents the weights between e th hidden neuron and the output neuron. b represents the bias weight values.

Model 1	2–17-1				
Input – > Hidden weights	Value	Hidden – > Output weights	Value	Bias weights	Value
$w_{i1,1}$	24.5454	w_{h1}	53.0008	$b_{i,h1}$	−29.5571
$w_{i1,2}$	26.3037	w_{h2}	−52.9212	$b_{i,h2}$	−32.2153
$w_{i1,3}$	−25.6890	w_{h3}	2.1435	$b_{i,h3}$	2.1383
$w_{i1,4}$	12.5770	w_{h4}	0.3687	$b_{i,h4}$	0.4506
$w_{i1,5}$	5.7434	w_{h5}	1.4505	$b_{i,h5}$	−15.6411
$w_{i1,6}$	−1.5639	w_{h6}	−118.2130	$b_{i,h6}$	1.0434
$w_{i1,7}$	−77.2897	w_{h7}	0.1585	$b_{i,h7}$	28.9941
$w_{i1,8}$	−1.5409	w_{h8}	116.8895	$b_{i,h8}$	1.0212
$w_{i1,9}$	178.5355	w_{h9}	1.9931	$b_{i,h9}$	−11.2990
$w_{i1,10}$	−11.3322	w_{h10}	0.6730	$b_{i,h10}$	−3.6433
$w_{i1,11}$	−865.1596	w_{h11}	−0.9479	$b_{i,h11}$	−1040.3193
$w_{i1,12}$	1.1087	w_{h12}	−31.3370	$b_{i,h12}$	−1.7869
$w_{i1,13}$	0.6733	w_{h13}	29.6269	$b_{i,h13}$	−1.3146
$w_{i1,14}$	14.7650	w_{h14}	−0.9269	$b_{i,h14}$	14.9359
$w_{i1,15}$	−97.5930	w_{h15}	0.2626	$b_{i,h15}$	−66.4042
$w_{i1,16}$	17.0872	w_{h16}	1.0520	$b_{i,h16}$	16.9196
$w_{i1,17}$	−45.1990	w_{h17}	−1.1072	$b_{i,h17}$	−28.0474
$w_{i2,1}$	−37.4360			$b_{h,o1}$	−2.5310
$w_{i2,2}$	−40.6760				
$w_{i2,3}$	4.6033				
$w_{i2,4}$	−9.8986				
$w_{i2,5}$	28.5628				
$w_{i2,6}$	−3.2334				
$w_{i2,7}$	88.7901				
$w_{i2,8}$	−3.4061				
$w_{i2,9}$	−20.9957				
$w_{i2,10}$	−16.6050				
$w_{i2,11}$	−887.8953				
$w_{i2,12}$	3.7221				
$w_{i2,13}$	3.4845				
$w_{i2,14}$	12.0743				
$w_{i2,15}$	6.2323				
$w_{i2,16}$	−15.3671				
$w_{i2,17}$	36.3800				

Model 2	4–17-1				
Input – > Hidden weights	Value	Hidden – > Output weights	Value	Bias weights	Value
$w_{i1,1}$	−13.4128	w_{h1}	−6.9021	$b_{i,h1}$	20.1366
$w_{i1,2}$	69.5996	w_{h2}	−9.2683	$b_{i,h2}$	−43.8286
$w_{i1,3}$	−18.9131	w_{h3}	−9.3557	$b_{i,h3}$	−5.8784
$w_{i1,4}$	−21.5742	w_{h4}	−10.4730	$b_{i,h4}$	−5.2833
$w_{i1,5}$	3.6529	w_{h5}	92.4102	$b_{i,h5}$	−0.8590
$w_{i1,6}$	3.9138	w_{h6}	7.9365	$b_{i,h6}$	5.2593
$w_{i1,7}$	−5.8049	w_{h7}	9.9186	$b_{i,h7}$	3.0563
$w_{i1,8}$	10.1468	w_{h8}	−7.1390	$b_{i,h8}$	−7.7154
$w_{i1,9}$	−1.4821	w_{h9}	−46.5277	$b_{i,h9}$	−0.1635
$w_{i1,10}$	−43.7605	w_{h10}	12.1636	$b_{i,h10}$	−13.2635
$w_{i1,11}$	−139.6637	w_{h11}	−10.5375	$b_{i,h11}$	−48.5314
$w_{i1,12}$	41.5387	w_{h12}	−6.9651	$b_{i,h12}$	−10.6831
$w_{i1,13}$	−24.8255	w_{h13}	−1.2412	$b_{i,h13}$	−8.5294
$w_{i1,14}$	0.5884	w_{h14}	−207.3682	$b_{i,h14}$	−5.9397
$w_{i1,15}$	12.5260	w_{h15}	−10.5267	$b_{i,h15}$	10.5123
$w_{i1,16}$	6.8413	w_{h16}	16.9567	$b_{i,h16}$	−1.8064
$w_{i1,17}$	0.0173	w_{h17}	−78.5614	$b_{i,h17}$	3.9655
$w_{i2,1}$	−3.9844			$b_{h,o1}$	1.7849
$w_{i2,2}$	−67.9396				
$w_{i2,3}$	−3.6723				
$w_{i2,4}$	16.6944				
$w_{i2,5}$	24.7525				
$w_{i2,6}$	3.9397				
$w_{i2,7}$	2.3348				
$w_{i2,8}$	4.0133				
$w_{i2,9}$	−18.4123				
$w_{i2,10}$	17.3751				
$w_{i2,11}$	150.0810				
$w_{i2,12}$	−5.3408				
$w_{i2,13}$	−10.5279				
$w_{i2,14}$	7.8761				
$w_{i2,15}$	−6.2984				
$w_{i2,16}$	−4.2162				
$w_{i2,17}$	−4.0494				
$w_{i3,1}$	16.3793				
$w_{i3,2}$	39.7687				
$w_{i3,3}$	−2.1102				
$w_{i3,4}$	−36.3029				
$w_{i3,5}$	−0.0010				
$w_{i3,6}$	3.8601				
$w_{i3,7}$	4.9267				
$w_{i3,8}$	−2.1556				
$w_{i3,9}$	4.6908				
$w_{i3,10}$	17.5709				
$w_{i3,11}$	44.4665				
$w_{i3,12}$	−68.9712				
$w_{i3,13}$	4.3229				
$w_{i3,14}$	−9.5568				
$w_{i3,15}$	10.4015				
$w_{i3,16}$	−7.4852				
$w_{i3,17}$	5.9609				
$w_{i4,1}$	9.1957				
$w_{i4,2}$	−48.1396				
$w_{i4,3}$	4.8605				
$w_{i4,4}$	14.7972				
$w_{i4,5}$	8.3394				
$w_{i4,6}$	−12.9558				
$w_{i4,7}$	−1.0995				
$w_{i4,8}$	−6.5600				
$w_{i4,9}$	−2.1447				
$w_{i4,10}$	10.2069				
$w_{i4,11}$	−98.2163				
$w_{i4,12}$	50.7683				
$w_{i4,13}$	30.5324				
$w_{i4,14}$	1.8516				
$w_{i4,15}$	6.0430				
$w_{i4,16}$	6.9044				
$w_{i4,17}$	−1.8563				

Model 3	3–16-1				
Input – > Hidden weights	Value	Hidden – > Output weights	Value	Bias weights	Value
$w_{i1,1}$	0.7900	w_{h1}	16.6822	$b_{i,h1}$	−1.4334
$w_{i1,2}$	−2.4405	w_{h2}	49.2759	$b_{i,h2}$	3.3807
$w_{i1,3}$	3.6484	w_{h3}	0.8780	$b_{i,h3}$	19.7109
$w_{i1,4}$	5.3563	w_{h4}	37.3675	$b_{i,h4}$	−5.2818
$w_{i1,5}$	−0.6495	w_{h5}	17.6630	$b_{i,h5}$	1.3619
$w_{i1,6}$	−72.5787	w_{h6}	−0.1434	$b_{i,h6}$	46.1625
$w_{i1,7}$	−38.3409	w_{h7}	2.2601	$b_{i,h7}$	−15.7929
$w_{i1,8}$	−6.0982	w_{h8}	−0.3572	$b_{i,h8}$	−32.0429
$w_{i1,9}$	−54.1103	w_{h9}	−2.3176	$b_{i,h9}$	−18.9087
$w_{i1,10}$	−5.7708	w_{h10}	−0.2439	$b_{i,h10}$	−9.8284
$w_{i1,11}$	−127.2051	w_{h11}	0.5985	$b_{i,h11}$	−48.7672
$w_{i1,12}$	−1.8687	w_{h12}	8.5480	$b_{i,h12}$	−6.3558
$w_{i1,13}$	−186.3715	w_{h13}	−0.5208	$b_{i,h13}$	−140.3256
$w_{i1,14}$	9.8503	w_{h14}	34.5651	$b_{i,h14}$	21.7480
$w_{i1,15}$	9.6640	w_{h15}	−34.4505	$b_{i,h15}$	21.5004
$w_{i1,16}$	107.1460	w_{h16}	0.7448	$b_{i,h16}$	70.9630
$w_{i2,1}$	−2.8825			$b_{h,o1}$	−6.2492
$w_{i2,2}$	2.2297				
$w_{i2,3}$	−11.8250				
$w_{i2,4}$	−3.6698				
$w_{i2,5}$	2.5375				
$w_{i2,6}$	−93.5044				
$w_{i2,7}$	−17.2936				
$w_{i2,8}$	155.9323				
$w_{i2,9}$	−34.0693				
$w_{i2,10}$	15.6145				
$w_{i2,11}$	70.0472				
$w_{i2,12}$	1.4655				
$w_{i2,13}$	201.8939				
$w_{i2,14}$	34.6580				
$w_{i2,15}$	31.3117				
$w_{i2,16}$	9.9501				
$w_{i3,1}$	0.4185				
$w_{i3,2}$	−0.0250				
$w_{i3,3}$	−18.4521				
$w_{i3,4}$	−0.6264				
$w_{i3,5}$	−0.3165				
$w_{i3,6}$	159.8662				
$w_{i3,7}$	−15.1827				
$w_{i3,8}$	−69.5745				
$w_{i3,9}$	−18.9240				
$w_{i3,10}$	−8.4678				
$w_{i3,11}$	77.3739				
$w_{i3,12}$	−2.6853				
$w_{i3,13}$	34.0073				
$w_{i3,14}$	16.3259				
$w_{i3,15}$	16.7612				
$w_{i3,16}$	−90.1044				

Model 4	5–17-1				
Input − > Hidden weights	Value	Hidden − > Output weights	Value	Bias weights	Value
$w_{i1,1}$	13.7500	w_{h1}	−0.9239	$b_{i,h1}$	6.4909
$w_{i1,2}$	−0.7709	w_{h2}	19.7344	$b_{i,h2}$	0.2661
$w_{i1,3}$	−0.3239	w_{h3}	−1.4382	$b_{i,h3}$	−0.4001
$w_{i1,4}$	−10.7179	w_{h4}	0.7592	$b_{i,h4}$	9.7379
$w_{i1,5}$	11.1386	w_{h5}	62.2222	$b_{i,h5}$	9.4112
$w_{i1,6}$	1.8852	w_{h6}	−3.7162	$b_{i,h6}$	−2.9139
$w_{i1,7}$	169.1636	w_{h7}	−0.2269	$b_{i,h7}$	−91.8204
$w_{i1,8}$	10.7503	w_{h8}	−3.8240	$b_{i,h8}$	4.1891
$w_{i1,9}$	1.6929	w_{h9}	10.6077	$b_{i,h9}$	−0.1087
$w_{i1,10}$	−0.1908	w_{h10}	28.4342	$b_{i,h10}$	−1.6608
$w_{i1,11}$	−145.3294	w_{h11}	−0.4848	$b_{i,h11}$	66.7425
$w_{i1,12}$	0.2320	w_{h12}	3.3686	$b_{i,h12}$	5.2978
$w_{i1,13}$	−1.4091	w_{h13}	−3.3799	$b_{i,h13}$	1.3047
$w_{i1,14}$	1.6539	w_{h14}	7.7633	$b_{i,h14}$	1.8888
$w_{i1,15}$	−11.4396	w_{h15}	62.1762	$b_{i,h15}$	−9.8357
$w_{i1,16}$	0.0913	w_{h16}	−15.3731	$b_{i,h16}$	−1.1867
$w_{i1,17}$	−0.0493	w_{h17}	2.7430	$b_{i,h17}$	−1.9396
$w_{i2,1}$	−3.5861			$b_{h,o1}$	20.5706
$w_{i2,2}$	4.4755				
$w_{i2,3}$	−8.2747				
$w_{i2,4}$	11.6187				
$w_{i2,5}$	−2.2330				
$w_{i2,6}$	−3.6574				
$w_{i2,7}$	−41.2862				
$w_{i2,8}$	−0.4749				
$w_{i2,9}$	−6.4735				
$w_{i2,10}$	−0.6306				
$w_{i2,11}$	−59.1514				
$w_{i2,12}$	2.2262				
$w_{i2,13}$	−2.4748				
$w_{i2,14}$	0.3647				
$w_{i2,15}$	2.2587				
$w_{i2,16}$	3.7542				
$w_{i2,17}$	6.7550				
$w_{i3,1}$	7.7338				
$w_{i3,2}$	−0.9117				
$w_{i3,3}$	4.9327				
$w_{i3,4}$	−9.9073				
$w_{i3,5}$	−10.2620				
$w_{i3,6}$	15.3007				
$w_{i3,7}$	68.1754				
$w_{i3,8}$	−5.2661				
$w_{i3,9}$	2.2737				
$w_{i3,10}$	0.2750				
$w_{i3,11}$	61.6855				
$w_{i3,12}$	9.3196				
$w_{i3,13}$	0.6738				
$w_{i3,14}$	0.3637				
$w_{i3,15}$	10.1394				
$w_{i3,16}$	−2.5260				
$w_{i3,17}$	−6.6621				
$w_{i4,1}$	−6.6177				
$w_{i4,2}$	−2.1425				
$w_{i4,3}$	−4.0999				
$w_{i4,4}$	−3.2918				
$w_{i4,5}$	2.7698				
$w_{i4,6}$	−12.8636				
$w_{i4,7}$	245.9058				
$w_{i4,8}$	−7.9421				
$w_{i4,9}$	2.7643				
$w_{i4,10}$	0.6082				
$w_{i4,11}$	252.8239				
$w_{i4,12}$	−4.4059				
$w_{i4,13}$	1.9564				
$w_{i4,14}$	−1.6445				
$w_{i4,15}$	−2.8750				
$w_{i4,16}$	−2.6125				
$w_{i4,17}$	−6.1548				
$w_{i5,1}$	−9.8102				
$w_{i5,2}$	0.2696				
$w_{i5,3}$	10.6313				

(*Continued*)

(Continued).

Model 4	5–17-1				
Input – > Hidden weights	Value	Hidden – > Output weights	Value	Bias weights	Value
$w_{i5,4}$	−0.7861				
$w_{i5,5}$	28.9900				
$w_{i5,6}$	−0.2034				
$w_{i5,7}$	−272.7526				
$w_{i5,8}$	−7.5603				
$w_{i5,9}$	−0.8357				
$w_{i5,10}$	0.3571				
$w_{i5,11}$	78.9411				
$w_{i5,12}$	0.9428				
$w_{i5,13}$	1.1416				
$w_{i5,14}$	−1.4136				
$w_{i5,15}$	−29.6400				
$w_{i5,16}$	−0.3737				
$w_{i5,17}$	0.8451				